Analysis of nonlocal thermodynamic equilibrium CO 4.7 μm fundamental, isotopic, and hot band emissions measured by the Michelson Interferometer for Passive Atmospheric Sounding on Envisat

B. Funke,[1] M. López-Puertas,[1] D. Bermejo-Pantaleón,[1] T. von Clarmann,[2] G. P. Stiller,[2] M. Höpfner,[2] U. Grabowski,[2] and M. Kaufmann[3]

Received 17 August 2006; revised 10 January 2007; accepted 28 February 2007; published 9 June 2007.

[1] Nonlocal thermodynamic equilibrium (non-LTE) simulations of the $^{12}C^{16}O(1 \rightarrow 0)$ fundamental band, the $^{12}C^{16}O(2 \rightarrow 1)$ hot band, and the isotopic $^{13}C^{16}O(1 \rightarrow 0)$ band performed with the Generic Radiative Transfer and non-LTE population Algorithm (GRANADA) and the Karlsruhe Optimized and Precise Radiative Transfer Algorithm (KOPRA) have been compared to spectrally resolved 4.7 μm radiances measured by the Michelson Interferometer for Passive Atmospheric Sounding (MIPAS). The performance of the non-LTE simulation has been assessed in terms of band radiance ratios in order to avoid a compensation of possible non-LTE model errors by retrieval errors in the CO abundances inferred from MIPAS data with the same non-LTE algorithms. The agreement with the measurements is within 5% for the fundamental band and within 10% for the hot band. Simulated $^{13}C^{16}O$ radiances agree with the measurements within the instrumental noise error. Solar reflectance at the surface or clouds has been identified as an important additional excitation mechanism for the CO(2) state. The study represents a thorough validation of the non-LTE scheme used in the retrieval of CO abundances from MIPAS data.

Citation: Funke, B., M. López-Puertas, D. Bermejo-Pantaleón, T. von Clarmann, G. P. Stiller, M. Höpfner, U. Grabowski, and M. Kaufmann (2007), Analysis of nonlocal thermodynamic equilibrium CO 4.7 μm fundamental, isotopic, and hot band emissions measured by the Michelson Interferometer for Passive Atmospheric Sounding on Envisat, *J. Geophys. Res.*, *112*, D11305, doi:10.1029/2006JD007933.

1. Introduction

[2] Carbon monoxide (CO) is an important atmospheric constituent. Besides methane oxidation and anthropogenic emissions, its main chemical source is located in the mesosphere and thermosphere by photodissociation of CO_2, leading to a pronounced volume mixing ratio (VMR) increase with altitude above the tropopause. This concentration gradient coupled with a long chemical lifetime make CO an excellent tracer for dynamical studies in the middle atmosphere. Apart from measurements in the microwave (i.e., SMR on Odin [*Dupuy et al.*, 2004] or MLS on Aura [*Filipiak et al.*, 2005]), the $CO(1 \rightarrow 0)$ and $CO(2 \rightarrow 0)$ ro-vibrational transitions at 4.7 and 2.4 μm are used to derive CO concentrations by remote sensing experiments. In contrast to solar occultation techniques used by ATMOS [*Newchurch et al.*, 1996] and recently by ACE-FTS [*Clerbaux et al.*, 2005], measurements of CO from atmospheric infrared emissions, though offering the advantage of global, illumination-independent coverage, are sparse. One of the reasons is that the retrieval of CO from its infrared emissions has to account for strong nonlocal thermodynamic equilibrium (non-LTE) effects, most pronounced at daytime, demanding sophisticated and time-consuming non-LTE retrieval schemes. Such CO non-LTE retrieval schemes have been applied to ISAMS measurements [*López-Valverde et al.*, 1996] and, more recently, to MIPAS observations.

[3] Several non-LTE population models for the $^{12}C^{16}O(1)$ state have been developed so far [*Winick et al.*, 1990; *López-Puertas et al.*, 1993]. Other models include also the $^{12}C^{16}O(2)$ level [*Kutepov et al.*, 1997] and isotopic $^{13}C^{16}O$ state distributions [*López-Valverde et al.*, 2005; *Dodd et al.*, 1993]. While the collisional schemes used in these models are similar, different non-LTE radiative transfer schemes (i.e., Curtis matrix method or lambda iteration) have been applied, however, without significant alteration of the resulting non-LTE populations.

[4] The accuracy of CO retrieval from 4.7 μm non-LTE emissions strongly depends on the accuracy of the non-LTE population model included. In contrast to ISAMS, the high

[1]Instituto de Astrofísica de Andalucía, Consejo Superior de Investigaciones Cientficas, Granada, Spain.
[2]Institut für Meteorologie und Klimaforschung, Forschungszentrum Karlsruhe und Universität Karlsruhe, Karlsruhe, Germany.
[3]Institut für Chemie und Dynamik der Geosphäre, Institut I: Stratosphäre, Forschungszentrum Jülich, Jülich, Germany.

0148-0227/07/2006JD007933

spectral resolution of MIPAS (0.035 cm^{-1}) allows for separation of different ro-vibrational CO lines and contaminant emissions, thus enabling for the first time the quantitative analysis of non-LTE emissions from the $^{12}C^{16}O$ ($1 \rightarrow 0$) fundamental band, the $^{12}C^{16}O(2 \rightarrow 1)$ hot band, and the isotopic $^{13}C^{16}O(1 \rightarrow 0)$ band. Such a quantitative analysis is required for a thorough validation of modeled CO populations. CO hot band emissions have not been observed directly in the Earth's atmosphere so far, although they have been detected on Titan with the ISAAC spectrometer at the Very Large Telescope [*López-Valverde et al.*, 2005]. In order to achieve an overall agreement of simulated and measured CO fundamental and hot band emissions on Titan, these authors proposed a CO-N_2 vibration-vibration (V-V) collisional rate constants 50% lower than those measured by *Allen and Simpson* [1980], commonly used in the CO non-LTE modeling. Fundamental band emissions of $^{13}C^{16}O$ and $^{12}C^{18}O$ have been observed with the CIRRIS instrument in the mesosphere and thermosphere [*Dodd et al.*, 1993]. Emissions of these minor isotopes were found to be up to 30 times more intense than predicted, based solely on the natural isotopic fractionation. This has been explained by a stronger radiative excitation of the minor isotopes due to a more effective absorption of tropospheric upwelling fluxes than by the main isotope.

[5] We employ the Generic Radiative Transfer and non-LTE population Algorithm GRANADA [*Funke et al.*, 2002] included in the Karlsruhe Optimized and Precise Radiative Transfer Algorithm (KOPRA) [*Stiller et al.*, 2002] to analyze MIPAS spectra in the 4.7 μm region and to validate the non-LTE modeling of CO vibrational populations. These algorithms are also used in the nonoperational retrieval of CO abundances from MIPAS (B. Funke et al., manuscript in preparation, 2007). In contrast to previous models, GRANADA includes also the near-infrared (NIR) albedo as additional daytime excitation mechanism which appears to be particularly important for the $^{12}C^{16}O(2)$ populations.

[6] The main goal of this paper is to validate calculated CO radiances by comparison to MIPAS measured radiances. After a description of the MIPAS measurements, we document the non-LTE simulations and assess their sensitivity to different collisional and radiative non-LTE parameters. Then we discuss the simulated radiances with respect to the radiance measurements. The subsequent validation on CO non-LTE radiance modeling is based on day/night, isotopic, and fundamental/hot band radiance ratios, since retrieved CO abundances depend on the non-LTE radiative transfer modeling, implying that direct intercomparison of absolute radiances would not allow any conclusive validation.

2. MIPAS Observations

[7] MIPAS is a limb emission Fourier transform spectrometer operating in the mid infrared spectral region. It has been designed for measurement of atmospheric trace species from space [*European Space Agency*, 2000; *Fischer and Oelhaf*, 1996]. It is part of the instrumentation of the Environmental Satellite (ENVISAT) which was launched into its Sun-synchronous polar orbit of 98.55° inclination at about 800 km altitude on 1 March 2002. MIPAS operated from July 2002 to March 2004 at full spectral resolution of 0.035 cm^{-1} (unapodized) in terms of full width at half maximum and with reduced resolution since August 2004. MIPAS observes the atmosphere during day and night with global coverage from pole to pole. Within its standard observation mode at full spectral resolution, MIPAS covers the altitude range from 6 to 68 km with tangent altitudes from 6 to 42 km every 3 km, and further tangent altitudes at 47, 52, 60, and 68 km. Occasionally, MIPAS also operates in several upper atmospheric modes scanning up to 170 km. MIPAS passes the equator in southerly direction at 10.00 am local time 14.3 times a day. During each orbit up to 72 limb scans are recorded. The Level-1b processing of the data, including processing from raw data to calibrated phase-corrected and geolocated radiance spectra, is performed by the European Space Agency (ESA) [*Nett et al.*, 1999].

[8] In this study we focus on the spectral range of 2020–2220 cm^{-1}. Since hot band and isotopic emissions from a single observation are close to the noise equivalent spectral radiance (NESR) of 4 nW/(cm^2 sr cm^{-1}), averaging of spectra is required. The averaging has been performed within measurements at comparable atmospheric conditions (i.e., pressure, temperature and constituent abundances), further separating between day and night observations. This allows for the analysis of night/day radiance ratios which are constrained rather by the relative non-LTE populations than by the CO VMR, thus being very valuable for the validation of non-LTE models. Since CO as dynamical tracer shows a very compact correlation with potential vorticity over a wide altitude range, equivalent latitudes (EqL) at MIPAS geolocations can be used as criterion for selection of ensembles of measurements at comparable atmospheric conditions. It should be noted that tidal effects might introduce differences in the CO VMR between day and night above approximately 70 km. This, however, affects only marginally night/day radiance ratios from measurements taken in the nominal observation mode (uppermost tangent height 68 km) since the vertical redistribution of CO due to tides above 70 km does not change significantly the radiance at lower tangent heights.

[9] We concentrate here on measurements taken between 19 and 27 September 2002 in the nominal mode with a total amount of more than 6000 limb scans. Four EqL bands have been defined by making use of ECMWF potential vorticities. This selection represents a trade-off between maximum number of measurements and minimum variance of temperature and CO VMR within each band. Only measurements fulfilling the EqL criterion at all altitudes simultaneously have been included in the selection. Additionally, we performed a similar selection for measurements in the upper atmospheric (UA) mode taken on 11 June 2003. These observations include limb scans up to 100 km and allow thus for the analysis of non-LTE radiances in the mesosphere and lower thermosphere. Because of the small number of available UA measurements, including only 270 limb scans, a less restrictive grouping of observations by the EqL criterion has been applied. A summary of selected EqL boxes is given in Table 1.

[10] Examples of coadded daytime and nighttime spectra taken in the nominal mode at 30 and 68 km tangent height are shown in Figure 1 (top and middle). While at 30 km, CO emissions are partly masked by contributions of O_3 (2020–2135 cm^{-1}) and N_2O (2170–2220 cm^{-1}), they dominate

Table 1. Equivalent Latitude Boxes Used in This Study

Box Number	Measurement Period	Observation Mode	Equivalent Latitude	Number of Scans (Day/Night)	SZA(°) at Day	Cloud Coverage, %	Mean Cloud Top Height, km	NIR Albedo, %
1	19–27 Sep 2002	nominal	61–34°S	71/48	34–80	83	3.6	19
2	19–27 Sep 2002	nominal	5°S–10°N	59/55	25–27	62	3.8	17
3	19–27 Sep 2002	nominal	10–29°N	67/55	27–38	59	5.6	15
4	19–27 Sep 2002	nominal	60–88°N	277/250	56–80	63	1.9	18
5	11 Jun 2003	upper atmosphere	90–40°S	20/–	70–90	81	4.5	17
6	11 Jun 2003	upper atmosphere	20°S–30°N	23/–	23–53	63	4.5	15

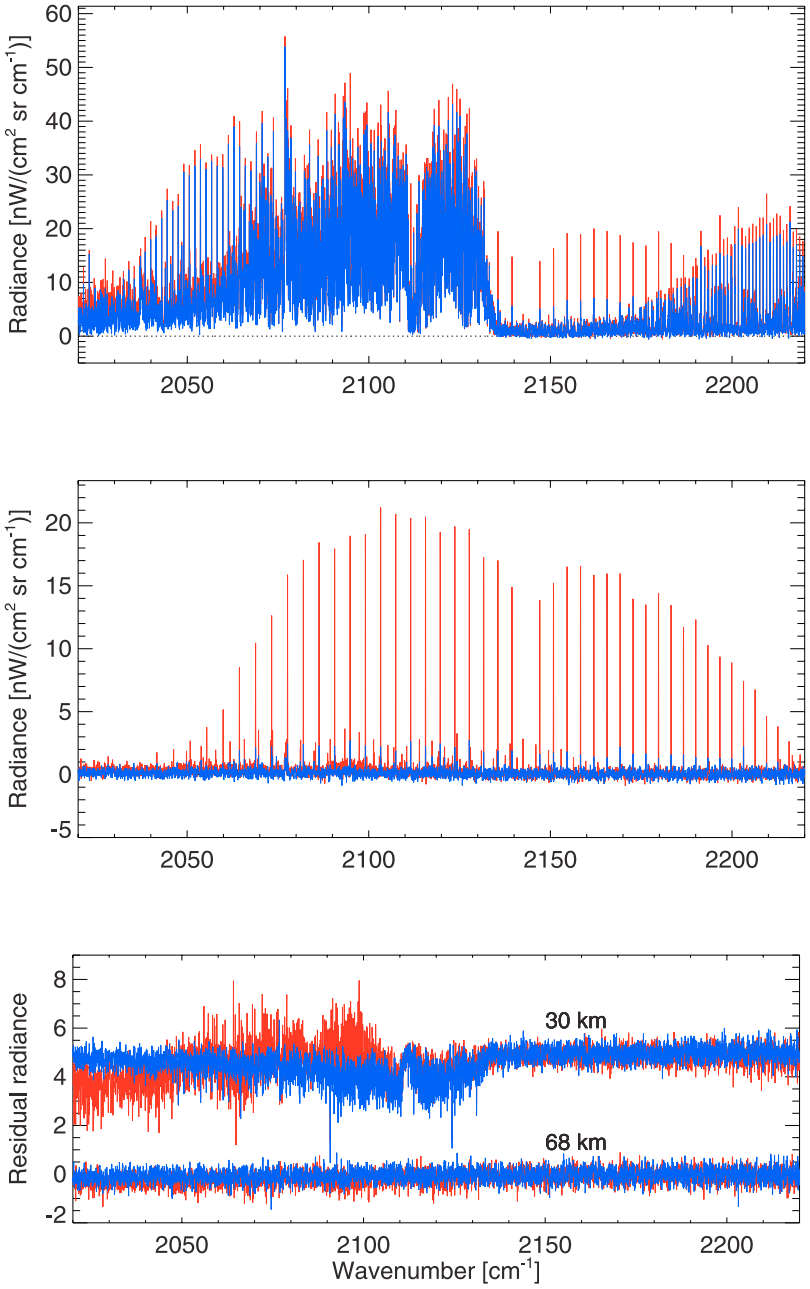

Figure 1. Coadded daytime (red) and nighttime (blue) MIPAS spectra around 4.7 μm measured at equivalent latitudes 10–29°N (box 3) on 19–27 September 2002 at tangent heights (top) 30 km and (middle) 68 km. (bottom) Simulated minus measured radiances for the same equivalent latitudes and tangent heights. Radiance differences for 30 km tangent height are shifted by 5 nW/(cm^2 sr cm^{-1}) for clarity. The NESR of the coadded spectra is 0.4 nW/(cm^2 sr cm^{-1}).

Table 2. Principal Collisional Processes Affecting the CO Vibrational States

Number	Process	Rate Coefficient[a]
1	$CO(v) + N_2 \rightleftharpoons CO(v-1) + N_2(1)$	$5.47 \times 10^{-15} \exp(3.82\,A - 5.47\,B)$
2	$CO(v) + O_2 \rightleftharpoons CO(v-1) + O_2(1)$	$9.79 \times 10^{-17} \exp(8.02\,A - 2.05\,B)$
3	$CO(v) + O(^3P) \rightleftharpoons CO(v-1) + O(^3P)$	$2.85 \times 10^{-14} \exp(9.50\,A + 1.11\,B)$

[a]Rate coefficient for the forward sense of the process in $cm^3\ s^{-1}$. $A = (T - 300) \times 10^{-3}$. $B = (T - 300)^2 \times 10^{-5}$. T is temperature in K.

the spectral region under consideration at 68 km. There, hot band and isotopic contributions can be identified in the daytime spectrum at 2040–2160 cm^{-1} with intensities about 10 times smaller than the dominating fundamental band. Nighttime fundamental band emissions are 40% of those during day at 30 km and only 10% at 68 km.

3. Non-LTE Simulations

[11] Limb radiances at 4.7 μm have been simulated with KOPRA in the 2020–2220 cm^{-1} regime including non-LTE emissions of CO_2, O_3, N_2O, CO, and continuum emissions of N_2. Vibrational populations of these gases have been calculated with GRANADA. This generic non-LTE algorithm provides vibrational and rotational non-LTE populations for relevant atmospheric IR emitters by solving iteratively the statistical equilibrium (SEE) and radiative transfer equations (RTE) under consideration of radiative, collisional and chemical excitation processes. The iteration scheme, i.e., the order of solutions of SEE and RTE, can be chosen by the user, allowing for Curtis matrix, lambda iteration, or mixed applications. Radiative transfer can be treated either line-by-line or by statistical band methods. Solar incoming fluxes at the top of the atmosphere are adapted from the SOLAR2000 solar irradiance model [*Tobiska et al.*, 2000], including modulations due to variations of the Sun-Earth distance. Attenuation of the solar flux by Fraunhofer lines is taken into account [*Hase et al.*, 2006]. NIR solar reflectance at the surface or clouds is considered assuming isotropic hemispheric reflection characterized by the NIR albedo. Tropospheric upwelling fluxes are calculated under consideration of surface emissions, tropospheric absorbing species and clouds, the latter characterized by the mean cloud top altitude and cloud coverage. Surface and cloud emissions are treated as blackbody radiation at the temperature of their respective height level.

[12] Non-LTE vibrational populations of CO are affected by radiative processes (spontaneous emission, absorption of solar radiation, and exchange of photons with the atmosphere and with the surface) and collisions with O_2, N_2, and O. The CO non-LTE modeling is performed for the $^{12}C^{16}O(v \leq 2)$ and $^{13}C^{16}O(v = 1)$ vibrational levels using lambda iteration and line-by-line radiative transfer. During daytime, CO vibrational populations are largely controlled by absorption of solar radiation at 4.7 and 2.4 μm. Solar CO Fraunhofer lines reduce significantly the solar incoming radiation at the CO ro-vibrational line positions. Typically, calculated reduction factors of the solar flux are around 0.7 for the $^{12}C^{16}O(v \rightarrow v-1)$ bands, and 0.95 for the overtone band at 2.4 μm and the fundamental bands of the minor isotopes. At nighttime, the absorption of tropospheric upwelling radiation determines the CO non-LTE populations. Collisional processes included in our nominal calculations are summarized in Table 2. We use rate constants for CO-O reported by *Lewittes et al.* [1978], for CO-N_2 those reported by *Allen and Simpson* [1980], and for CO-O_2 those measured by *Doyennette et al.* [1977]. These quenching rates, though measured for $^{12}C^{16}O(v = 1)$, are also applied to $^{12}C^{16}O(v = 2)$ and $^{13}C^{16}O(v = 1)$. While no more recent laboratory measurements of rate constants for CO-N_2 collisions are available, *Wang et al.* [1998] measured CO-O_2 vibration-vibration (V-V) rates which are 2 orders of magnitude faster than those reported by *Doyennette et al.* [1977]. Because of the collisional coupling of $CO(v = 1,2)$ with $N_2(v = 1)$ and $CO_2(v_3)$ via V-V energy transfer, non-LTE populations of the latter molecules are calculated first. The CO_2 and N_2 vibrational populations have been modeled using the Curtis matrix method including the collisional processes reported by *López-Puertas and Taylor* [2001] with updates for CO_2 [*López-Puertas et al.*, 2005]. N_2O has been modeled as described by *López-Puertas et al.* [2007]. For O_3, the steady state equation is solved using a revised collisional scheme and nascent distribution [*Kaufmann et al.*, 2005].

[13] The limb radiance simulations have been performed for average atmospheric and instrumental conditions of the MIPAS measurements taken in the nominal mode during 19–27 September 2002 and in the upper atmospheric mode on 11 June 2003 for each of the EqL boxes described in the previous section (see Table 1). Instrumental line of sight, pressure, temperature, and VMRs of O_3, N_2O, CO, and CH_4 were retrieved first from all measurements using the IMK/IAA scientific data processor [*von Clarmann et al.*, 2003]. Except for CO, all quantities have been averaged separately for daytime and nighttime observations. By using a mean CO VMR independent on day and night conditions and by analyzing night/day radiance ratios rather than absolute radiances, a compensation of possible non-LTE model errors mapped into the retrieved CO abundances has been avoided. CO VMR retrievals were performed under consideration of non-LTE, using a non-LTE model setup identical to that described here as nominal.

[14] Mean cloud coverage and top altitudes have been taken from the International Satellite Cloud Climatology Project (ISCCP) monthly averaged D2 products (http://isccp.giss.nasa.gov/). NIR surface albedos have been calculated using the ISCCP vegetation classification and specific NIR albedos from the Aster Spectral library (http://speclib.jpl.nasa.gov/). NIR cloud albedos have been estimated from the ISCCP cloud coverage and cloud optical depths in the Visible, assuming a dependence of reflectivity on optical depth in the Visible at a typical effective droplet radius of 10 μm as reported by *Chang and Li* [2002]. Average NIR albedos for all EqL boxes have than been determined as the

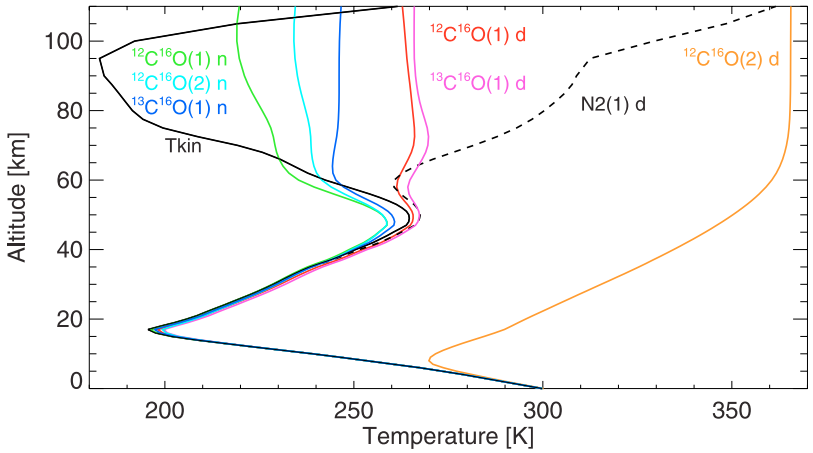

Figure 2. Kinetic and modeled vibrational temperature (VT) profiles for the $^{12}C^{16}O(1)$, $^{12}C^{16}O(2)$, and $^{13}C^{16}O(1)$ vibrational levels for mean atmospheric conditions at equivalent latitudes 10–29°N (EqL box 3) during day (d) and night (n). Daytime VTs for $N_2(1)$ are also shown.

sum of cloud and surface albedos weighted with the cloud and clear sky fractions, respectively. A summary of cloud and NIR albedo related parameters is given in Table 1.

[15] The dependence of CO daytime vibrational populations on the solar zenith angle (SZA) is nonlinear, particularly for the $^{12}C^{16}O(1)$ state. Since the SZA variance is rather large in some EqL boxes, the radiance contributions for each EqL box have been calculated for 5° SZA bins and subsequently weighted with the number of measurements within each SZA bin.

[16] Figure 2 shows vibrational temperature (VT) profiles for the $^{12}C^{16}O(1)$, $^{12}C^{16}O(2)$, and $^{13}C^{16}O(1)$ vibrational levels for mean atmospheric conditions at equivalent latitudes 10–29°N during day and night. While $^{12}C^{16}O(2)$ daytime populations are far away from LTE at all altitudes, the effect of solar excitation during day is most pronounced above 50 km for CO(1) states. However, VTs of CO(1) are up to 10 K below the kinetic temperature at 40–50 km during night, while they exceed the kinetic temperature by 2–3 K during day below 50 km. In order to assess the impact of relevant collisional and radiative non-LTE parameters on the vibrational state distribution, we performed additional calculations with different sets of non-LTE parameters. Figure 3 shows VT differences with respect to the nominal case for (1) calculations with $CO\text{-}O_2$ V-V rates of *Wang et al.* [1998], (2) reduced $CO\text{-}N_2$ V-V rates by a factor of 2, (3) clear-sky conditions, and (4) without consideration of the NIR albedo. The effect of applying the $CO\text{-}O_2$ rate of *Wang et al.* [1998] is less than 3 K for the CO(1) states but reaches 7 K for $C^{16}O^{12}(2)$ below 50 km during day. The use of this rate generally reduces the difference of VT and kinetic temperature. The effect of a

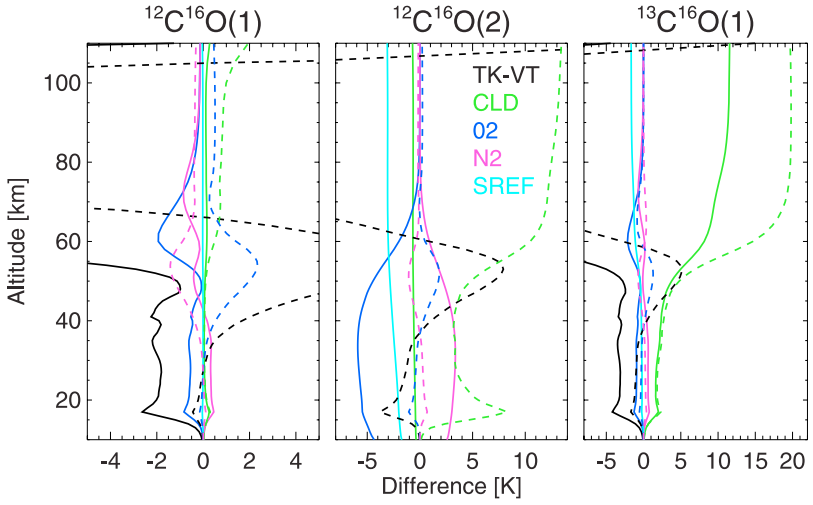

Figure 3. Vibrational temperature (VT) differences (deviation from nominal VTs) for the (left) $^{12}C^{16}O(1)$, (middle) $^{12}C^{16}O(2)$, and (right) $^{13}C^{16}O(1)$ vibrational levels during day (solid lines) and night (dashed lines) for atmospheric conditions as in Figure 2 due to assumption of cloud-free conditions (CLD), use of the $CO\text{-}O_2$ rate constant of *Wang et al.* [1998] (O2), reduction of the $CO\text{-}N_2$ rate constant by a factor of 2 (N2), and neglect of solar reflectance (SREF). Differences between kinetic and vibrational temperatures (TK-VT) are also shown.

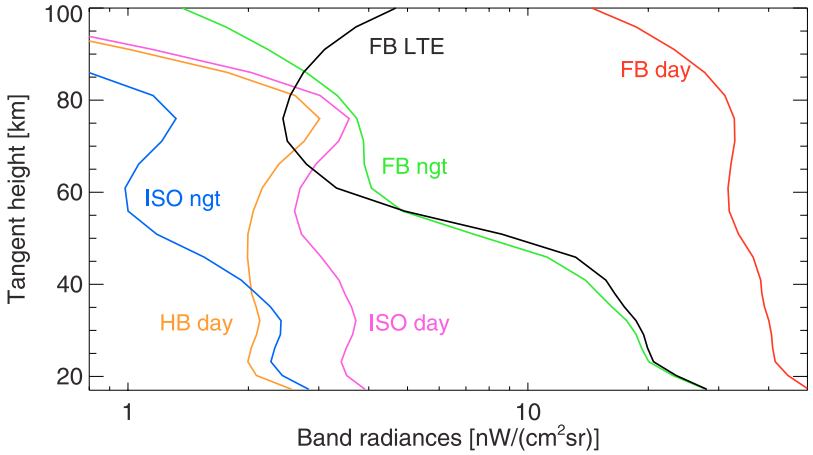

Figure 4. Simulated band non-LTE radiances over tangent height for the fundamental (FB), hot (HB), and isotopic (ISO) CO bands during day and night for atmospheric conditions as in Figure 2, using nominal non-LTE populations. LTE radiances of the fundamental band are also shown.

reduced CO-N_2 rate is less than 2 K for the CO(1) states and reaches 4 K for CO(2) below 50 km. Except for the CO(1) states at daytime, non-LTE deviations are enhanced by the reduced CO-N_2 rate. Lower daytime VTs of CO(1) above 50 km are due to a less effective V-V energy transfer from N_2(1) which is strongly excited during day (see Figure 2). The neglect of clouds has an important impact on the $^{13}C^{16}O$(1) populations in the mesosphere, enhancing their VTs by up to 12 and 20 K during day and night, respectively. This is in agreement with the finding of *Dodd et al.* [1993] that isotopic fundamental band emissions are largely controlled by absorption of the upwelling tropospheric flux. A similar sensitivity to clouds is found for the $^{12}C^{16}O$(2) nighttime populations. The neglect of the NIR albedo reduces daytime VTs of this state by about 3 K, while its impact on other states is negligible.

[17] Integrated daytime and nighttime band radiances calculated with the nominal VTs are shown in Figure 4. Nighttime hot band radiances have been omitted since they are below the detection limit of MIPAS. In agreement with the measured 4.7 μm spectra shown in Figure 1, isotopic and hot band radiances are approximately one order of magnitude smaller than the fundamental band daytime radiances. Nighttime fundamental band radiances are smaller than at daytime by a factor of 2 and 10 in the stratosphere and mesosphere, respectively. The effect of variations in the VTs on the different band radiances is shown in Figure 5. The application of the CO-O_2 rate of *Wang et al.* [1998] has a small effect (<3%) on the daytime fundamental band radiances and isotopic radiances at both day and night, but leads to significant enhancements of nighttime fundamental band radiances (up to 7% at 50 km) and daytime hot band radiances (13% at 20 km). A 50%

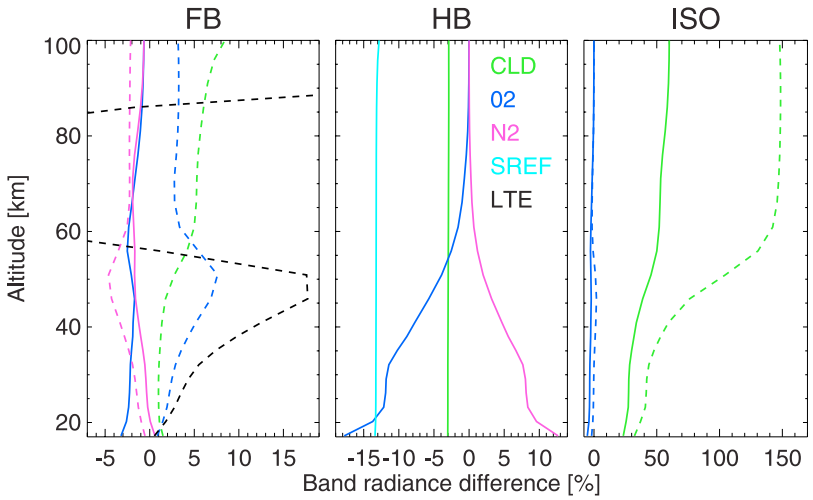

Figure 5. Relative radiance differences (deviation from nominal calculations) for the (left) fundamental, (middle) hot, and (right) isotopic CO bands for mean atmospheric conditions as in Figure 2 due to assumption of cloud-free conditions (CLD), use of the CO-O_2 rate constants of *Wang et al.* [1998] (O2), reduction of CO-N_2 rate constant by a factor of 2 (N2), and neglect of solar reflectance (SREF) at day (solid lines) and night (dashed lines). Radiance differences which do not exceed 2% have been omitted. Differences due to assumption of LTE are shown for nighttime fundamental band radiances.

reduction of the CO-N_2 rate has an opposite and smaller effect (<4% for the fundamental band during night and <10% for the hot band during day). The neglect of clouds enhances isotopic radiances by up to 50% and 100% during day and night, respectively, while the effect on the fundamental band is rather small (5% at night and 1% at day, not shown). A 3% decrease of daytime hot band radiances due to assumption of cloud-free conditions is related to an indirect cloud effect on the NIR albedo. The neglect of solar reflectance at the surface or clouds decreases these radiances by 13%.

[18] In order to assess the feasibility of less time-consuming LTE retrievals of CO from nighttime fundamental band radiances, we have also performed LTE calculations of this band. These calculations overestimate nighttime radiances by up to 20% below 50 km and deviate by more than 50% above. Hence the assumption of LTE in the retrieval of CO would introduce considerable systematic errors even at nighttime conditions.

4. Non-LTE Spectra and CO Band Radiances

[19] In a first step, simulated 4.7 μm non-LTE radiances using the nominal VTs are compared to coadded measured spectra. Figure 1 (bottom) shows radiance differences between simulated and coadded measured daytime and nighttime spectra for equivalent latitudes 10–29°N (box 3). At 30 km, residual radiances at wavenumbers greater than 2135 cm^{-1} are close to the noise level, but differences in the order of 2–3 nW/(cm^2 sr cm^{-1}) appear at lower wavenumbers which are most probably related to the non-LTE modeling of O_3 highly excited vibrational levels. This problem is currently being resolved by refinements of the non-LTE scheme of O_3. At 68 km, the agreement between simulations and measurements is excellent.

[20] For calculation of CO band mean radiance contributions in the measured and simulated spectra, we restrict ourselves to the 2135–2200 cm^{-1} spectral region which is less affected by emissions from other species. Fundamental band contributions have been averaged from 0.15 cm^{-1} wide spectral intervals around the P1, P2, and R0–R23 lines, subtracting the contributions of emissions not belonging to this band. These have been determined by means of simulations with the fundamental band source function set to zero. A similar procedure has been applied to the hot band R5–R12 lines and to the isotopic band R11–R24 lines, excluding in the latter case R14, R17, and R20.

[21] Instrumental noise errors of the measured mean band radiance contributions are within 0.015–0.06 nW/(cm^2 sr cm^{-1}). Apart from potential errors introduced by CO vibrational temperatures, modeled band radiance contributions are mainly affected by uncertainties in the CO VMRs used. The CO VMR, however, is retrieved from the measured fundamental band radiances under investigation, and the CO retrieval error budget is dominated by measurement noise. Therefore model errors due to CO VMR uncertainties may well contribute to the simulated radiances error budget but not to the difference between modeled and measured fundamental band radiances. This is not the case for isotopic and hot band emissions. However, because of their one order of magnitude smaller intensity, their related forward model errors are small compared to the measurement noise error.

[22] A further forward model error source is the uncertainty of the kinetic temperature, which has been estimated to be less than 3%. Possible model errors due to uncertainties in the isotope fractionation of CO might affect $^{13}C^{16}O$ band radiances. However, these uncertainties have been estimated to be smaller than 5% [*Dodd et al.*, 1993], much less than the measurement noise error in this band. The simplified treatment of the lower boundary conditions in the non-LTE modeling by representing surface and clouds as blackbody radiators introduces negligible errors in the band radiance contributions of the $^{12}C^{16}O$ isotope and errors less than 7% in the $^{13}C^{16}O$ fundamental band radiances.

[23] It should be noted that the comparison of simulated spectra calculated from linearly averaged atmospheric and instrumental parameters with coadded measurements might also suffer from errors due to nonlinear radiative transfer. However, the variance of atmospheric and instrumental parameters (except for SZA) within each EqL box is generally comparable to their uncertainties at a single location. Thus it is not expected that the averaging introduces significant additional errors compared to the rigorous approach of coadding simulations for each measurement location which would require an enormous computational effort. Errors related to the use of average cloud statistics have been explicitly assessed by a sensitivity study including calculations for various cloud altitudes. The errors in mesospheric CO populations, introduced by the nonlinear dependence on cloud altitude, are negligible for the main isotope (v = 1,2), but are in the order of 1–10% for the $^{13}C^{16}O$(v = 1) state (depending on the cloud top height distribution assumed). However, related errors in simulated $^{13}C^{16}O$ band radiances are well below the measurement noise error.

[24] Figure 6 shows measured and simulated mean radiance contributions of the fundamental, hot, and isotopic bands for observations on 19–27 September 2002 at equivalent latitudes 10–29°N (EqL box 3) for both day and night conditions. The overall agreement for all bands is very good and differences are generally below the precision of the measurements. Isotopic contributions are, however, close to the noise level which is due to the restriction to the 2135–2200 cm^{-1} spectral region which includes mainly transitions involving high-J levels.

[25] Figure 7 shows measured and simulated daytime mean radiance contributions for two EqL boxes corresponding to UA observations on 11 June 2003 extending up to 100 km. As for the lower altitudes, the agreement between measurements and simulations is very good also in the 70–100 km region for all CO bands. At polar winter conditions (EqL box 5), high mesospheric and stratospheric CO abundances are responsible for enhanced hot and isotopic band radiances leading to an excellent signal to noise ratio, while the fundamental band contribution does not change significantly with respect to tropical conditions (EqL box 6). The higher hot/fundamental band ratio at polar winter conditions is caused by stronger attenuation of the solar flux at higher SZAs which affects particularly the fundamental band.

5. Model Validation

[26] A quantitative comparison of non-LTE effects in simulated and measured CO emissions is best performed

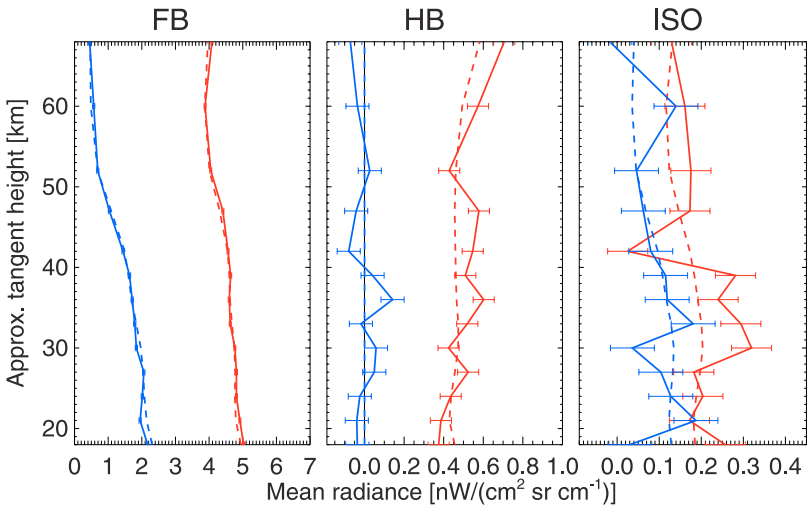

Figure 6. Observed (solid lines) and simulated (dashed lines) mean radiances contributions of the fundamental (FB), hot (HB) and isotopic (ISO) CO bands at equivalent latitudes 10–29°N (EqL box 3) during day (red) and night (blue). Error bars represent the noise error of the coadded measurements (hardly visible for the fundamental band).

in terms of band radiance ratios since they are less influenced by the CO abundances than the radiances themselves. Ratios of fundamental band night/day radiances, hot/fundamental band daytime radiances, as well as isotopic/fundamental band radiances during both day and night have been determined for all EqL boxes of the nominal measurements from 19 to 27 September 2002. Figure 8 shows the simulated night/day radiance ratios of the fundamental band. Band radiance ratios at tropical equivalent latitudes are generally higher than at midlatitude or polar latitudes between 25 and 50 km which can be explained by higher stratospheric kinetic temperatures in the tropics. Nighttime VTs of CO(1), being closer to LTE, depend more strongly on the kinetic temperature than the daytime VTs. The overall agreement of simulations and measurements is within 5%. Simulations show, however, a positive bias below 50 km and a small negative bias above. Although these differences exceed the measurement noise error only marginally, we have checked if they could be caused by deficiencies in the non-LTE modeling. An overestimation of the cloud altitude or coverage could introduce a low bias of less than 5% above 50 km but could not explain the differences below. The use of the CO-O_2 rate of *Wang et al.* [1998] would increase the band radiance ratio by 5–10% which would cause worse agreement below 50 km. On the other hand, a reduction of simulated radiance ratios could be obtained by decreasing the collisional rates. Since the nominal CO-O_2 rate is too slow to noticeably affect CO(1) populations, a reduction of the radiance ratio could only be achieved by using a lower CO-N_2 rate. When reducing it by 50%, we obtained a decrease in the simulated radiance ratios of up to 3% around 45 km, but considerably

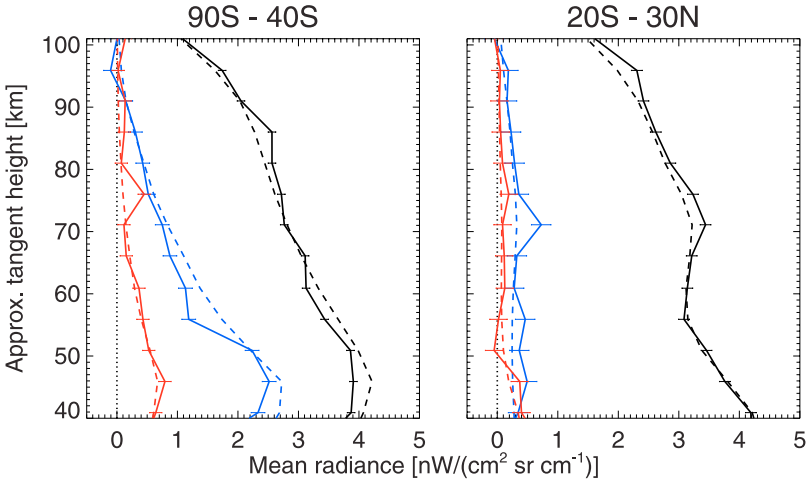

Figure 7. Observed (solid lines) and simulated (dashed lines) mean daytime radiances contributions of fundamental (black), hot (blue), and isotopic (red) CO bands at equivalent latitudes (left) 90–40°S and (right) 20°S–30°N (EqL boxes 5 and 6) on 11 June 2003. Error bars represent the noise error of the coadded measurements.

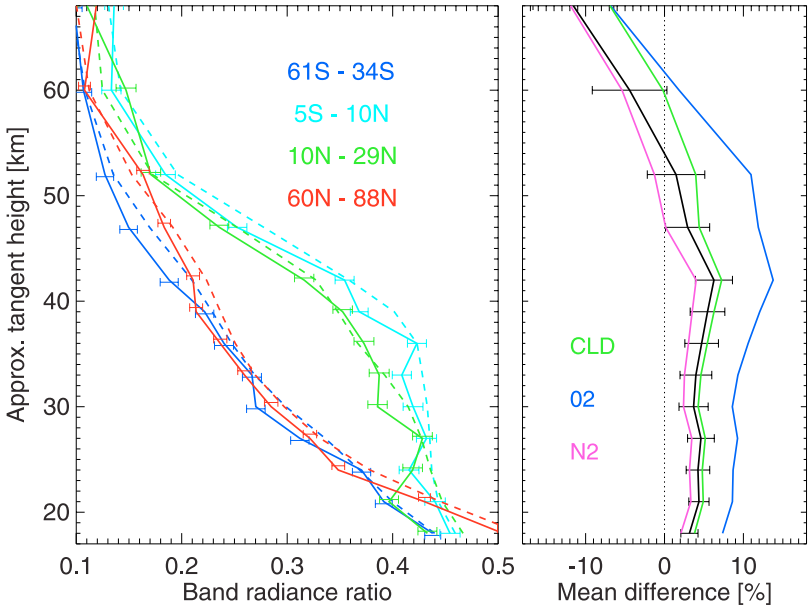

Figure 8. (left) Measured (solid lines) and simulated (dashed lines) ratios of nighttime and daytime radiances of the fundamental CO band at all equivalent latitude (EqL) boxes (different colors) on 19–27 September 2002. (right) Mean of the differences of the measured and calculated band radiance ratios for nominal non-LTE parameters (black), assumption of cloud-free conditions (CLD), use of the CO-O_2 rate constants of *Wang et al.* [1998] (O2), and reduction of CO-N_2 rate constant by a factor of 2 (N2). Error bars represent the noise error of the coadded measurements.

smaller differences at other altitudes. Hence reducing the CO-N_2 V-V rate by 50%, as proposed by *López-Valverde et al.* [2005],would get a better overall agreement although would not fully explain the observed differences.

[27] Contrary to the fundamental band night/day ratio, the radiance ratio of the daytime hot/fundamental band increases toward higher latitudes in both hemispheres (see Figure 9), which is due to a stronger reduction of solar excitation of the CO(1)level at high SZAs (see Table 1) compared to CO(2). Highest hot/fundamental band ratios are found in the Southern Hemisphere where CO abundances are enhanced by meridional transport. In this case, spectral saturation limits the intensity of the fundamental band while hot band emissions increase linearly with the CO VMR. In the mean, simulations agree with the measurements within 10%, showing a negative bias above 35 km.

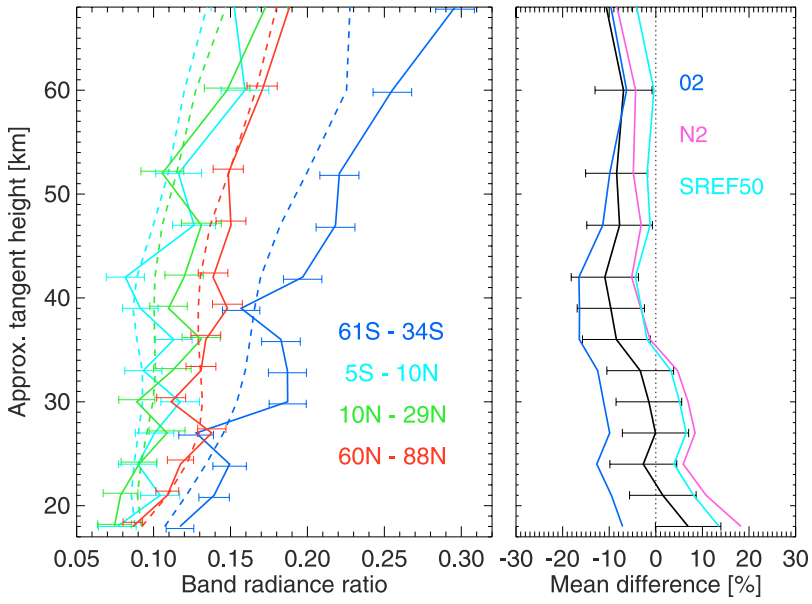

Figure 9. Same as Figure 8 but for the ratios of hot/fundamental band daytime radiances. The curve labeled SREF50 in the right plot refers to an enhancement of the NIR albedo by 50%.

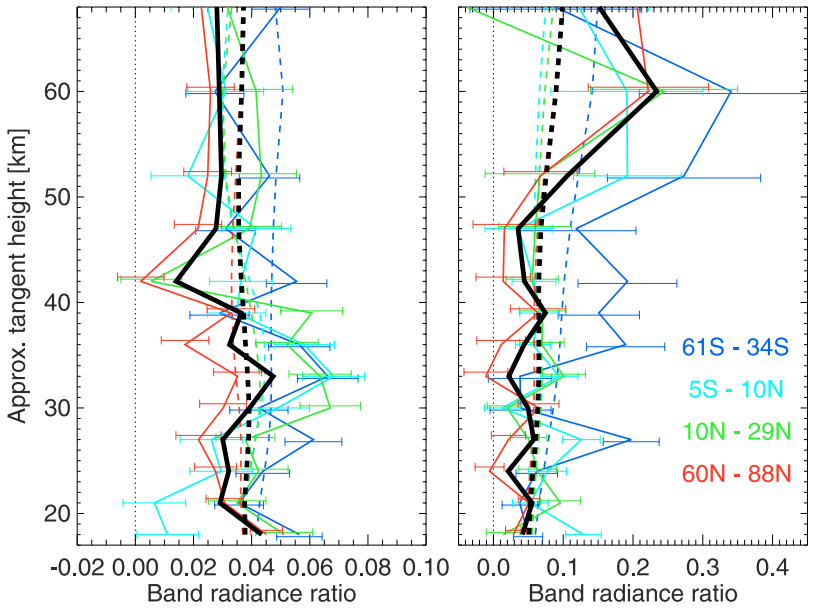

Figure 10. Measured (solid lines) and simulated (dashed lines) ratios of isotopic and fundamental band radiances at (left) daytime and (right) nighttime for all equivalent latitude boxes (different colors) on 19–27 September 2002. The average ratios for all equivalent latitude boxes are shown by the thick solid and dashed lines. Error bars represent the noise error of the coadded measurements.

Also in this case, the effect of clouds on the band radiance ratio is too small to explain the remaining differences. The impact of collisional processes on this radiance ratio is most pronounced at altitudes below 50 km. Both, application of the CO-O_2 rate of *Wang et al.* [1998] and a reduced CO-N_2 rate introduce changes in the order of 10%, resulting in decreased (increased) ratios in the first (latter) case. While worse agreement is obtained at all altitudes by using the modified CO-O_2 rate, the application of the 50% reduced CO-N_2 rate leads to better agreement above 35 km although overestimates the measurements by 10–20% below. An underestimation of the NIR albedo could explain the low bias of the simulations above 35 km, although would introduce a slight overestimation below. Thus an increase of the NIR albedo in the order of 50% would give a better overall agreement.

[28] The measured $C^{16}O^{13}/C^{16}O^{12}$ ratios of $1 \rightarrow 0$ band radiances are close to the noise level which makes their analysis in terms of non-LTE effects difficult. However, the impact of clouds on these radiance ratios is very strong, introducing changes of 50–100%. Since simulated radiance ratios agree reasonably well with the measurements (see Figure 10), there is no hint on model deficiencies with respect to the attenuation of tropospheric upwelling radiances by clouds.

6. Conclusions

[29] We have used spectrally resolved MIPAS 4.7 μm radiances in order to validate calculations of non-LTE emissions from the $^{12}C^{16}O(1 \rightarrow 0)$ fundamental band, the $^{12}C^{16}O(2 \rightarrow 1)$ hot band, and the isotopic $^{13}C^{16}O(1 \rightarrow 0)$ band which has been performed with the GRANADA non-LTE population model and the KOPRA radiative transfer code. The performance of the non-LTE simulation has been assessed in terms of band radiance ratios in order to avoid a compensation of possible non-LTE model errors mapped into the retrieved CO abundances. On the other hand, the assessment of radiance ratios does not allow for detection of non-LTE model errors which scale day and night band radiances in the same way. However, we found that simulated radiance ratios are sensitive to changes in the magnitude of all relevant non-LTE processes (see Figure 8). The existence of an unknown non-LTE process which would cause a scaling of day and night populations by the same factor seems to be very unlikely.

[30] The agreement with the measurements is within 5% for the fundamental band and within 10% for the hot band. Differences exceed the measurement noise error only marginally. Collisional processes affecting CO vibrational states seem to be well described by the nominal non-LTE model setup including CO-N_2 V-V rates of *Allen and Simpson* [1980] and CO-O_2 V-V rates as described by *Doyennette et al.* [1977]. In particular, there is no evidence for a 100 times enhanced CO-O_2 rates as measured by *Wang et al.* [1998]. A reduction of the CO-N_2 rate by 50% as proposed by *López-Valverde et al.* [2005] introduces changes only in the order of the measurement noise error, although slightly improves the overall agreement of simulations and measurements. Hence no unequivocal conclusion can be drawn with respect to the proposed change of this rate. Solar reflectance at the surface or clouds has been identified as an important additional excitation mechanism for the CO(2) state. However, a low bias of up to 10% of simulated hot/fundamental band radiance ratio with respect to the measurements hints on an underestimation of the NIR albedo. Simulated $^{13}C^{16}O$ fundamental band radiances agree with the measurements within the instrumental noise error.

[31] Since CO non-LTE retrieval from MIPAS measurements are performed from fundamental band radiances

using the same non-LTE population and radiative transfer models as applied to this work, we conclude that the non-LTE scheme used in these retrievals is validated to an accuracy of 5%. While the need of a time-consuming non-LTE retrieval scheme for CO is evident at daytime conditions, we have further shown that the assumption of LTE in CO nighttime retrieval from 4.7 μm fundamental band emissions would introduce systematic model errors in the retrieved stratospheric CO abundances of 10–20%.

[32] **Acknowledgments.** The IAA team was supported by the Spanish project ESP2004-01556 and EC FEDER funds. The IMK team was partly supported by BmBF 50 EE 0512. The authors acknowledge ESA for providing MIPAS L1b spectra, as well as ECMWF for meteorological data.

References

Allen, D. C., and C. J. S. M. Simpson (1980), Vibrational energy exchange between CO and the isotopes of N_2 between 300 K and 80 K, *J. Chem. Phys.*, *45*, 203–211.

Chang, F.-L., and Z. Li (2002), Estimating the vertical variation of cloud droplet effective radius using multispectral near-infrared satellite measurements, *J. Geophys. Res.*, *107*(D15), 4257, doi:10.1029/2001JD000766.

Clerbaux, C., P.-F. Coheur, D. Hurtmans, B. Barret, M. Carleer, R. C. K. Semeniuk, J. C. McConnell, C. Boone, and P. Bernath (2005), Carbon momoxide distribution from the ACE-FTS solar occultation measurements, *Geophys. Res. Lett.*, *32*, L16S01, doi:10.1029/2005GL022394.

Dodd, J. A., J. R. Winick, W. A. M. Blumberg, S. J. Lipson, P. S. Armstrong, and J. R. Lowell (1993), CIRRIS 1A observations of $^{13}C^{16}O$ and $^{12}C^{18}O$ fundamental band radiance in the upper atmosphere, *Geophys. Res. Lett.*, *20*(23), 2683–2686.

Doyennette, L., G. Mastrocinque, A. Chakroun, H. Guenguen, M. Margottin-Maclou, and L. Henry (1977), Temperature dependence of the vibrational relaxation of CO (v = 1) by NO, O_2, and D_2, and of the self-relaxation of D_2, *J. Chem. Phys.*, *67*, 3360–3366.

Dupuy, E., et al. (2004), Strato-mesospheric measurements of carbon monoxide with the Odin sub-millimetre radiometer: Retrieval and first results, *Geophys. Res. Lett.*, *31*, L20101, doi:10.1029/2004GL020558.

European Space Agency (2000), Envisat, MIPAS: An instrument for atmospheric chemistry and climate research, *Eur. Space Agency Spec. Publ.*, *ESA SP-1229*.

Filipiak, M. J., et al. (2005), Carbon momoxide measured by the EOS Microwave Limb Sounder on Aura: First results, *Geophys. Res. Lett.*, *32*, L14825, doi:10.1029/2005GL022765.

Fischer, H., and H. Oelhaf (1996), Remote sensing of vertical profiles of atmospheric trace constituents with MIPAS limb-emission spectrometers, *Appl. Opt.*, *35*(16), 2787–2796.

Funke, B., F. J. Martín-Torres, M. López-Puertas, M. Höpfner, F. Hase, M. Á. López-Valverde, and M. García-Comas (2002), A generic non-LTE population model for MIPAS–ENVISAT data analysis, *Geophys. Res. Abstr.*, *4*.

Hase, F., P. Demoulin, A. J. Sauval, G. C. Toon, P. F. Bernath, A. Goldman, J. W. Hannigan, and C. P. Rinsland (2006), An empirical line-by-line model for the infrared solar transmittance spectrum from 700 to 5000 cm^{-1}, *J. Quant. Spectrosc. Radiat. Transfer*, *102*, 450–463, doi:10.1016/j.jqsrt.2006.02.026.

Kaufmann, M., et al. (2005), Vibrationally excited ozone in the middle atmosphere, *J. Atmos. Sol. Terr. Phys.*, *68*(2), 125–244, doi:10.1016/j.jastp.2005.10.006.

Kutepov, A. A., H. Oelhaf, and H. Fischer (1997), Non-LTE radiative transfer in the 4.7 and 2.3 μm bands of CO: Vibration–rotational non-LTE and its effects on limb radiance, *J. Quant. Spectrosc. Radiat. Transfer*, *57*(3), 317–339.

Lewittes, M. E., C. C. Davis, and R. A. Farlane (1978), Vibrational deactivation of CO (v = 1) by oxygen atoms, *J. Chem. Phys.*, *69*, 1952–1957.

López-Puertas, M., and F. W. Taylor (2001), *Non-LTE radiative transfer in the Atmosphere*, World Scientific Pub., Singapore.

López-Puertas, M., M. Á. López-Valverde, D. P. Edwards, and F. W. Taylor (1993), Non-local-thermodynamic-equilibrium populations of the first vibrational excited state of CO in the middle atmosphere, *J. Geophys. Res.*, *98*(D5), 8933–8947.

López-Puertas, M., et al. (2005), Atmospheric non-local thermodynamic equilibrium emissions as observed by the Michelson Interferometer for Passive Atmospheric Sounding (MIPAS), *C. R. Phys.*, *6*(8), 848–863, doi:10.1016/j.crhy.2005.07.012.

López-Puertas, M., B. Funke, D. Bermejo-Pantaleón, T. von Clarmann, G. P. Stiller, U. Grabowski, and M. Höpfner (2007), Evidence for N_2O ν_3 4.5 μm non-local thermodynamic equilibrium emission in the atmosphere, *Geophys. Res. Lett.*, *34*, L02825, doi:10.1029/2006GL028539.

López-Valverde, M. Á., M. López-Puertas, J. J. Remedios, C. D. Rodgers, F. W. Taylor, E. C. Zipf, and P. W. Erdman (1996), Validation of measurements of carbon monoxide from the improved stratospheric and mesospheric sounder, *J. Geophys. Res.*, *101*(D6), 9929–9955.

López-Valverde, M. Á., E. Lellouch, and A. Coustenis (2005), Carbon monoxide fluorescence from Titan's atmosphere, *Icarus*, *175*, 503–521, doi:10.1016/j.icarus.2004.12.015.

Nett, H., B. Carli, M. Carlotti, A. Dudhia, H. Fischer, J.-M. Flaud, G. Perron, P. Raspollini, and M. Ridolfi (1999), MIPAS ground processor and data products, *Proc. IEEE Int. Geosci. Remote Sens. Symp. 1999*, *3*, 1692–1696.

Newchurch, M. J., et al. (1996), Stratospheric NO and NO_2 abundances from ATMOS solar-occultation measurements, *Geophys. Res. Lett.*, *23*(17), 2373–2376.

Stiller, G. P., T. von Clarmann, B. Funke, N. Glatthor, F. Hase, M. Höpfner, and A. Linden (2002), Sensitivity of trace gas abundances retrievals from infrared limb emission spectra to simplifying approximations in radiative transfer modelling, *J. Quant. Spectrosc. Radiat. Transfer*, *72*(3), 249–280.

Tobiska, W. K., T. Woods, F. Eparvier, R. Viereck, L. Floyd, D. Bouwer, G. Rottman, and O. R. White (2000), The SOLAR2000 empirical solar irradiance model and forecast tool, *J. Atmos. Terr. Phys.*, *62*, 1233–1250.

von Clarmann, T., et al. (2003), Retrieval of temperature and tangent altitude pointing from limb emission spectra recorded from space by the Michelson Interferometer for Passive Atmospheric Sounding (MIPAS), *J. Geophys. Res.*, *108*(D23), 4736, doi:10.1029/2003JD003602.

Wang, B., Y. Gu, and F. Kong (1998), Multilevel vibrational-vibrational (V-V) energy transfer from CO (ν) to O_2 and CO_2, *J. Phys. Chem. A*, *102*, 9367–9371.

Winick, J. R., P. P. Wintersteiner, and R. H. Picard (1990), Non-LTE emissions from CO (ν = 1) in the mesosphere and lower thermosphere and its effect on remote sensing, in *Digest of Topical Meeting on Optical Remote Sensing of the Atmosphere*, vol. 4, pp. 611–614, Opt. Soc. Am., Washington, D. C.

D. Bermejo-Pantaleón, B. Funke, and M. López-Puertas, Instituto de Astrofisica de Andalucía, Apartado Postal 3004, E-18080 Granada, Spain. (bernd@iaa.es)

M. Höpfner, U. Grabowski, G. P. Stiller, and T. von Clarmann, Institut für Meteorologie und Klimaforschung, Forschungszentrum Karlsruhe und Universität Karlsruhe, Postfach 3640, D-76021 Karlsruhe, Germany.

M. Kaufmann, Institut I: Stratosphäre, Institut für Chemie und Dynamik der Geosphäre Forschungszentrum Jülich, D-52425 Jülich, Germany.